# Delay feedback induces a spontaneous motion of two-dimensional cavity solitons in driven semiconductor microcavities

M. Tlidi,[1] E. Averlant,[1,3] A. Vladimirov,[2] and K. Panajotov[3,4]

[1]*Faculté des Sciences, Université Libre de Bruxelles (U.L.B.), Code Postal 231, Campus Plaine, Bruxelles B-1050, Belgium*

[2]*Weierstrass Institute for Applied Analysis and Stochastics, Mohrenstrasse 39, Berlin D-10117, Germany*

[3]*Department of Applied Physics and Photonics (IR-TONA), Vrije Unversiteit Brussels, Pleinlaan 2, Brussels B-1050, Belgium*

[4]*Institute of Solid State Physics, 72 Tzarigradsko Chaussee Boulevard, Sofia 1784, Bulgaria*

(Received 8 May 2012; published 18 September 2012)

We consider a broad area vertical-cavity surface-emitting laser (VCSEL) operating below the lasing threshold and subject to optical injection and time-delayed feedback. We derive a generalized delayed Swift-Hohenberg equation for the VCSEL system, which is valid close to the nascent optical bistability. We first characterize the stationary-cavity solitons by constructing their snaking bifurcation diagram and by showing clustering behavior within the pinning region of parameters. Then, we show that the delayed feedback induces a spontaneous motion of two-dimensional (2D) cavity solitons in an arbitrary direction in the transverse plane. We characterize moving cavity solitons by estimating their threshold and calculating their velocity. Numerical 2D solutions of the governing semiconductor laser equations are in close agreement with those obtained from the delayed generalized Swift-Hohenberg equation.

DOI: 10.1103/PhysRevA.86.033822 PACS number(s): 42.65.Tg, 42.65.Sf, 42.60.Da, 47.54.−r

## I. INTRODUCTION

During the past two decades, the study of localized structures, often called dissipative solitons or cavity solitons, has attracted considerable attention in many areas of natural science, such as chemistry, plant ecology, and optics (see recent overviews [1–5]). They attract growing interest in optics due to potential applications for all-optical control of light, optical storage, and information processing [6–12]. These stable localized objects arise in a dissipative environment and belong to the class of dissipative structures found far from equilibrium. Cavity solitons are stationary localized intensity peaks that appear in a subcritical regime, involving a homogeneous background of radiation and a self-organized periodic pattern, which are both linearly stable. They can be manipulated individually by the process of writing or erasing through an external control beam when they are sufficiently well separated from each other. When, however, the distance between peaks decreases, they start to interact through their oscillating exponentially decaying tails. This interaction then leads to the formation of clusters. Therefore, the number of peaks and their spatial distribution in the transverse plane can be either independent and randomly distributed or clustered forming a well-defined spatial pattern [13]. Recently, the relative stability analysis of different clusters of closely packed localized peaks has been performed [14].

Cavity solitons are not necessarily stationary objects. They can be time dependent, e.g., moving or oscillating. In particular, different mechanisms leading to the motion of dissipative solitons have been described in the literature. It has been shown that uniform motion of solitons can be induced by a vorticity [15], finite relaxation rates [16–18], a phase gradient [19], an Ising-Bloch transition [20–22], a walk-off, a symmetry breaking due to off-axis feedback [23], a resonator detuning [24], or a Hopf-Turing interacting bifurcation [25].

More recently, it has been shown that inclusion of delayed feedback in the dynamics of spatially extended systems can lead to a drift instability in cavity solitons [26]. This behavior has been identified first in the case when the delayed feedback is frequency selective [27–30]. Spontaneous motion of a single-cavity soliton in the case of non-frequency-selective (i.e., regular) feedback has been predicted in Ref. [26]. This result has been obtained with a model of a passive nonlinear cavity filled with two-level atoms without population inversion and driven coherently by an external injected beam. Other studies of various spatially extended systems with time delays have motivated further investigation of this subject [31].

In this paper, we investigate the effect of a regular delayed feedback on the mobility properties of two-dimensional (2D) cavity solitons in a broad area vertical-cavity surface-emitting faser (VCSEL). The delayed feedback is provided by an external mirror located at a distance $L_{\mathrm{ext}}$ from the output facet of the VCSEL. The structure of the considered device is schematically illustrated in Fig. 1. We assume that the laser operates in a single-longitudinal mode, the diffraction in the external cavity is fully compensated, and the feedback field is sufficiently attenuated so that it can be modeled by a single delay term with a spatially homogeneous coefficient. We show that this device can admit both stationary dissipative solitons and solitons moving in the transverse direction. Unlike a previous paper where the analysis is performed in strictly one transverse dimension [32], here, we consider the case of two transverse dimensions. We show that stationary-cavity solitons exhibit a clustering behavior, which has been experimentally observed in Ref. [33]. This behavior corresponds to back and forth oscillations of the laser output energy curve inside the pinning region. We explore the mechanism of the formation of localized structures by constructing their bifurcation diagram with changing amplitude of optical injection. We show that, when the strength of the delayed feedback exceeds some threshold value, two-dimensional cavity solitons exhibit a spontaneous motion in the laser transverse section.

The paper is organized as follows: In Sec. II, we introduce and discuss the VCSEL model. In Sec. III, in the neighborhood

 ©2012 American Physical Society

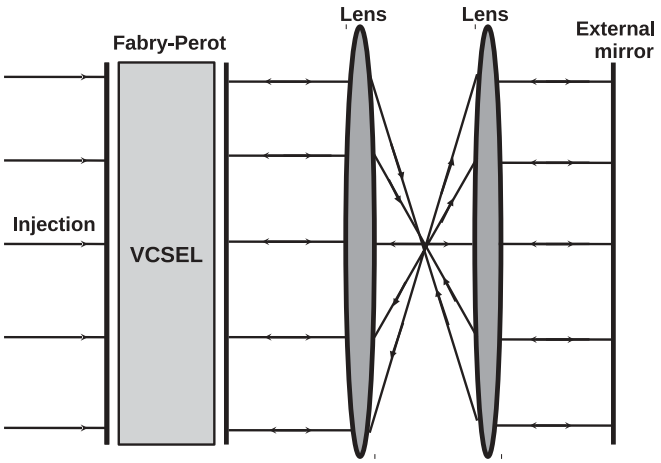


FIG. 1. Schematic setup of a Fabry-Pérot cavity with delayed optical feedback and driven by a coherent external injected beam. The nonlinear medium consists of a vertical-cavity surface-emitting laser. To compensate the diffraction in the external cavity, we use two lenses in a self-imaging configuration.

of the second-order critical point marking the onset of the hysteresis loop, we derive the generalized Swift-Hohenberg (SH) equation with time delays and perform a linear stability analysis of the spatially homogeneous stationary solutions of this equation. In Sec. IV, we describe the snaking bifurcation diagram associated with stationary-cavity solitons. Analytical calculations of the drift instability threshold as well as the velocity of moving solitons are obtained in this section. Finally, numerical simulations of the generalized Swift-Hohenberg equation with time delays are presented in Sec. IV together with the results of numerical integration on the original laser model. Concluding remarks are given in Sec. V.

## II. MEAN-FIELD MODEL OF A VCSEL WITH A TIME DELAY

The laser model under consideration is obtained from the scalar Maxwell-Bloch equations using the slowly varying envelope and paraxial approximations. We assume that the laser operates in a single-longitudinal mode. Under these approximations, the mean-field model describing the space-time evolution of the electric-field envelope $E$ and the normalized carrier density $Z$ in a broad area VCSEL subject to optical injection and delayed optical feedback is given by the following set of dimensionless partial-differential equations [32]:

$$\partial_{t'}E = -(1+i\theta)E + 2C(1-i\alpha)(Z-1)E + E_i + \xi e^{i\psi}E(t'-\tau') + i\nabla_\perp'^2 E, \quad (1)$$

$$\partial_{t'}Z = -\gamma'[Z - I + (Z-1)|E|^2 - d\nabla_\perp'^2 Z], \quad (2)$$

where $E_i$ is the amplitude of the injected beam. The parameter $\theta$ is the cavity detuning, $C$ is the bistability parameter, and $\alpha$ is the linewidth enhancement factor. The feedback is characterized by the time delay $\tau' = 2L_{\rm ext}/c$, the feedback strength $\xi = k_f/\kappa$, and phase $\psi$. Here, $L_{\rm ext}$ is the external cavity length; $c$ is the speed of light, and $k_f = (1-r^2)r_{\rm ext}/(r\tau_{\rm in})$ with $r$ and $r_{\rm ext}$, respectively, are the VCSEL output mirror and the external mirror amplitude reflectivities. $\tau_{\rm in} = 2L_C n_C/c$ is the VCSEL cavity round-trip time with $L_C$ and $n_C$ as the VCSEL effective cavity length and refractive index, respectively. The parameter $\gamma'$ is the carrier decay rate, $I$ is the injected current (we assume that the laser operates below the lasing threshold), and $d$ is the diffusion coefficient. The diffraction of light and diffusion of the carriers is described by the Laplace operator $\nabla_\perp'^2 = \partial^2_{x'x'} + \partial^2_{y'y'}$, acting on the transverse plane $(x', y')$. In the absence of delayed feedback $\xi = 0$, we recover the mean-field model of Ref. [34]. The linear stability analysis of the spatially homogeneous steady states of Eqs. (1) and (2) as well as the numerical analysis of stationary- and moving-cavity solitons have been performed in Ref. [32] in a strictly one-dimensional setting.

In order to reduce the number of free parameters, we introduce the following change in variables: $n = [2C(Z-1)-1]/2$ and $e = E^*/\sqrt{2}$. The model equations (1) and (2) of the semiconductor laser driven by an injected field $Y = E_i/(2\sqrt{2})$ take the following form:

$$\partial_t e = i\theta' e + (1+i\alpha)ne + Y + \eta' e^{-i\psi}e(t-\tau) - i\nabla_\perp^2 e, \quad (3)$$

$$\partial_t n = \gamma[P - n - (1+2n)|e|^2 + D\nabla_\perp^2 n]. \quad (4)$$

The pump parameter $P$ is $P = C(I-1) - 1/2$, $\gamma = \gamma'/2$, $D = 2d$, $\eta' = \xi/2$, and $\theta' = (\theta+\alpha)/2$. The new time and space scales are $(t,\tau) = 2(t',\tau')$ and $\nabla_\perp^2 = 2\nabla_\perp'^2$. Let us assume, for simplicity, that the detuning is $\theta' = 0$ and the feedback phases are $\psi = 0$ or $\psi = \pi$. The homogeneous steady states are solutions of the two coupled equations $Y = -e_s(1+i\alpha)(P-|e_s|^2)/(1+2|e_s|^2)$ and $n_s = (P-|e_s|^2)/(1+2|e_s|^2)$. It is well known that the dynamics of a driven semiconductor cavity exhibits Turing instability and hysteresis, the former giving rise to either periodic or localized patterns consisting of localized intensity pulses in the transverse plane. In order to obtain a qualitative picture of the dynamics of this system, we focus our analysis on the regime which is (i) close to the nascent bistability threshold where the phenomenon of slowing down occurs, i.e., $\partial Y/\partial|e_s| = \partial^2 Y/\partial|e_s|^2 = 0$ and (ii) close to the long-wavelength pattern-forming instability. In this regime, the space-time dynamics is governed by the well-known Swift-Hohenberg equations [35].

## III. DERIVATION OF THE GENERALIZED SWIFT-HOHENBERG EQUATION WITH A TIME DELAY

In this section, we explore the nascent optical bistability regime near the critical point where the output intensity as a function of the injection parameter $Y$ has an infinite slope, i.e., $\partial Y/\partial|e_s| = \partial^2 Y/\partial|e_s|^2 = 0$. The coordinates of the critical point are $e_c = (1-i\alpha)\sqrt{3/2(1+\alpha^2)}$, $n_c = -3/2$, $P_c = -9/2$, $D_c = 8\alpha/[3(1+\alpha^2)]$, and $Y_c = (3/2)^{(3/2)}(1+\alpha^2)^{1/2}$. We consider the large time-delay regime, and we assume that the amplitude of the feedback strength is small: $\eta' e^{-i\psi} = \eta\varepsilon^2$ and $\tau \to (1/\gamma + D_c/\alpha)\tau/\varepsilon^2$, where $\varepsilon$ is a small parameter and $\eta, \tau = O(1)$. The strength of the feedback $\eta$ is positive for $\psi = 0$ and is negative for $\psi = \pi$. We seek corrections to the steady-state solution at the criticality that depend on time and space via the slow variables $t \to (1/\gamma + D_c/\alpha)\varepsilon^2 t$ and $(x,y) \to (\varepsilon/D_c)^{1/2}(x,y)$. We

expand the input field amplitude $Y$, the parameter $P$, and the variables $e$ and $n$ around their critical values, $e = e_c(1 + \varepsilon u + \varepsilon^2 e_2 \cdots)$, $n = n_c(1 + \varepsilon n_1 + \varepsilon^2 n_2 \cdots)$, $Y = Y_c(1 - \varepsilon^2 p_2/2 + \varepsilon^3 y \cdots)$, $P = P_c(1 + 3\varepsilon^2 p_2 + \cdots)$, and $D = D_c(1 + \varepsilon d + \cdots)$. We substitute these expansions and the space-time scalings in Eqs. (3) and (4). We get $u = -n_1$ in the leading-order problem, i.e., $O(\epsilon)$ where $u$ has to be real. At the $O(\epsilon^2)$, we obtain $e_2 = -i\{\nabla_\perp^2 u/(4\alpha) + 2\eta\alpha/[3(1+\alpha^2)]\}$ and $n_2 = u^2 - p_2/2 - \nabla_\perp^2 n_1/4$. Finally, the solvability condition at $O(\epsilon^3)$ leads to the following delayed partial-differential equation:

$$\partial_t u = y - u(p + u^2) + \eta u(t - \tau) + \left(d - \frac{5u}{2}\right)\nabla_\perp^2 u - a\nabla_\perp^4 u - 2(\nabla_\perp u)^2, \quad (5)$$

where $a$ is $a = (1 - \alpha^2)/(4\alpha^2)$. Note that $y$ is the deviation from the injected field amplitude and denotes the transverse coordinate at the same time. The real variable $u$, the parameters $p$ and $d$ are the deviations of the electric field, the pump parameter, and the carrier diffusion coefficient from their values at the onset of the critical point, respectively. In the absence of delay, i.e., $\eta = 0$, Eq. (5) is the generalized Swift-Hohenberg equation that has been derived for many far-from-equilibrium systems [35,36]. The Eq. (5) model differs from the usual delayed Swift-Hohenberg equation [26,36] in two significant ways. First, the presence of nonlinear diffusion terms $u\nabla_\perp^2 u$ breaks the symmetry $u \mapsto -u$ and allows Eq. (5) to exhibit modulational instabilities with different wavelengths. Second, in the absence of delay, Eq. (5) is nonvariationally devoid of gradient form, and therefore, it does not admit a Lyapunov functional or a free energy to minimize. As a consequence, the cavity soliton could move with a constant velocity even in the absence of delayed feedback [36].

The homogeneous stationary solutions $u_s$ of Eq. (5) are given by $y = u_s(p - \eta + u_s^2)$. For $p < \eta$ ($p > \eta$), the transmitted intensity as a function of the input intensity is monostable (bistable). We now perform the linear stability analysis of the homogeneous steady states. The linear deviation from the steady state is proportional to $\exp(\lambda t + i\mathbf{q}\cdot\mathbf{r})$, where $\mathbf{r} = (x, y)$ stands for the transverse coordinates and the transverse wave vector is $\mathbf{q}$. The transcendental characteristic equation reads

$$\lambda = -(p + 3u_s^2) - q^2\left(d - \frac{5u_s}{2}\right) - \frac{(1-\alpha^2)}{4\alpha^2}q^4 + \eta e^{-\lambda\tau}. \quad (6)$$

Modulational instabilities correspond to the occurrence of the zero real root ($\lambda = 0$) and $\partial_q \lambda = 0$. Our calculations show that there can be zero, one, or two modulational instabilities. The critical wave number associated with both instabilities is as follows:

$$q_{T\pm}^2 = \frac{\alpha^2(5u_{T\pm} - 2d)}{(1-\alpha^2)}. \quad (7)$$

The threshold $u_{T\pm}$ associated with these instabilities is as follows:

$$u_{T\pm} = \frac{2[5\alpha^2 d \pm \sqrt{(1-\alpha^2)[\alpha^2(12d^2 - 37) + 12](p - \eta)}]}{12 - 37\alpha^2}. \quad (8)$$

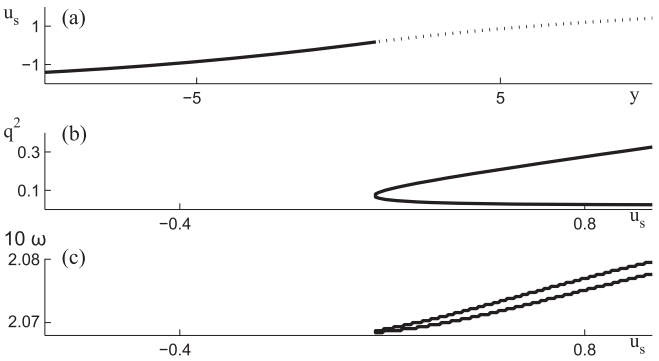


FIG. 2. Stability curves associated with traveling-wave instability in the monostable regime. The characteristics: (a) output field ($u_s$) as a function of input field ($y$), (b) wave number $q^2$, and (c) angular frequency $\omega$ are plotted as a function of output field ($u_s$). The full and the broken lines correspond to stable and unstable homogeneous steady states, respectively. Parameters are $p = 5$, $d = -1$, $a = 0.1$, $\eta = -0.1$, and $\tau = 15$.

The classifications of different scenarios leading to the instability of the homogeneous steady state are summarized in Ref. [37].

The linear stability analysis shows that there exists a Hopf bifurcation with a finite wave number often called traveling-wave instability. This instability occurs if a pair of complex conjugate roots of Eq. (6) has a vanishing real part and a nonzero imaginary part, i.e., $\lambda = \pm i\omega$. This instability occurs when

$$\eta\cos(\omega\tau) = (3u^2 + p) + \left(d - \frac{5u}{2}\right)q^2 + aq^4, \quad (9)$$

$$\eta\sin(\omega\tau) = -\omega. \quad (10)$$

Two examples of stability curves are shown in Figs. 2 and 3 where we plot the homogeneous steady states in the monostable and in the bistable regimes, the unstable wave numbers, and the unstable frequencies associated with the traveling-wave instability.

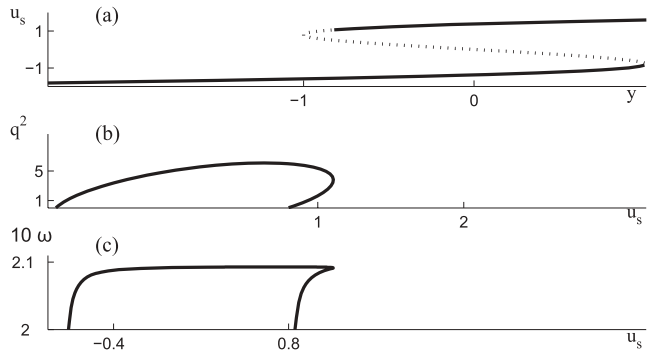


FIG. 3. Stability curves associated with traveling-wave instability in the bistable regime. The characteristics: (a) output field ($u_s$) as a function of input field ($y$), (b) wave number $q^2$, and (c) angular frequency $\omega$ are plotted as a function of output field ($u_s$). The full and the broken lines correspond to stable and unstable homogeneous steady states, respectively. Parameters are $p = -2$, $d = -1$, $a = 2$, $\eta = -0.1$, and $\tau = 15$.

## IV. STATIONARY AND MOVING LOCALIZED STRUCTURES

### A. Light clustering and moving-cavity solitons

In the case of one spatial dimension, stationary dissipative solitons correspond to the solutions of the Swift-Hohenberg equation homoclinic in space and stationary in time. The existence of an infinite set of homoclinic solutions in the variational Swift-Hohenberg equation has been demonstrated [38]. This behavior is referred to as the homoclinic snaking phenomenon [39]: The system exhibits a high degree of multistability in a finite range of parameters often called the pinning region. In this region, a stable homogeneous steady state coexists with a stable spatially periodic solution, and there is an infinite set of patterns comprising different numbers of cavity solitons. Each of them is characterized by either an odd or an even number of peaks. The configuration that maximizes the number of cavity solitons in the pattern corresponds to the spatially periodic distribution of the field amplitude. Examples of localized patterns having odd and even numbers of peaks are shown in Fig. 4. All localized patterns shown in these figures are obtained for the same parameter values and differ only by the initial condition. In the pinning region, the wavelength of the localized patterns is close to that of the periodic structure, i.e., $\lambda_{T+} \approx 2\pi/q_{T+}$. Since the peak amplitudes of localized patterns comprising different numbers of solitons are close to each other, it is convenient to plot the "$L_2$ norm" defined by the relation $N = \int dx|u - u_s|^2$ instead of the peak amplitudes. A typical bifurcation diagram, illustrating the dependence of $N$ on the input field amplitude $y$, is shown in Fig. 5. It consists of two snaking curves: one corresponding to localized patterns with an odd number of peaks and the other—to patterns

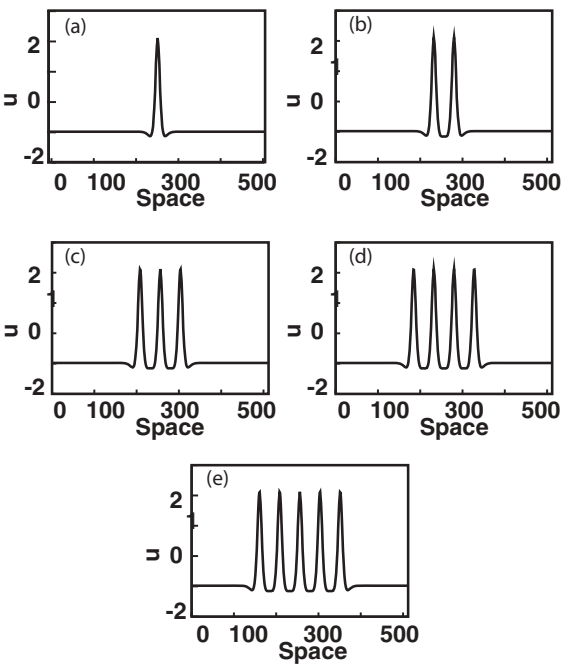


FIG. 4. Stationary localized patterns formed with one through five cavity solitons in the amplitude of the intracavity field. The parameters are $y = -0.35$, $p = -0.7$, $d = -1.2$, $a = 0.75$, $\tau = 1$, and $\eta = 0.1$.

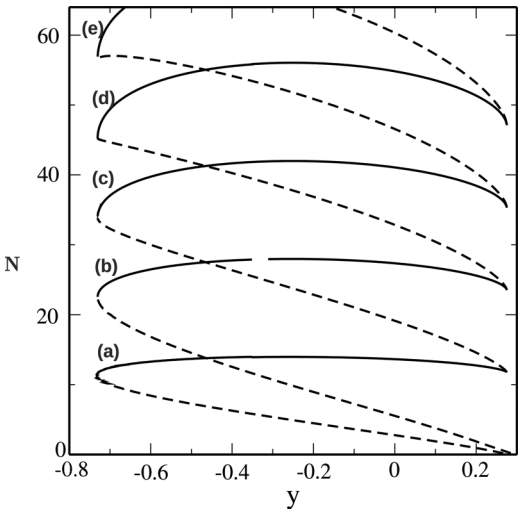


FIG. 5. Snaking bifurcation diagram of Eq. (5) showing two interweaved snaking curves: The branches (a)–(e) correspond to one through five cavity solitons, respectively (see Fig. 3). The full and the broken lines correspond to stable and unstable localized branches of solutions, respectively. The parameters are $p = -0.7$, $d = -1.2$, $a = 0.75$, and $\tau = \eta = 0$.

with an even number of peaks. The two interweaved snaking curves emerge from the modulation instability point located at $u = u_{T+}$. For each curve, as $N$ increases, at every turning point where the slope becomes infinite, a pair of additional peaks appears in the pattern. From Fig. 5, it is seen that this growth is associated with back and forth oscillations around the pinning region. In the case of a fiber ring resonator, diffraction is replaced by chromatic dispersion. In this context, localized structures are often called temporal-cavity solitons, which can also exhibit the homoclinic snaking phenomenon [40].

In the absence of feedback, all localized patterns, involving odd or even numbers of cavity solitons, are stationary. As we see in the next subsection, when the delayed feedback strength passes through the threshold value given by $\eta\tau = -1$, localized patterns start to move spontaneously in an arbitrary direction. This is due to the isotropy of space $(x, y)$. Examples of 1D and 2D moving patterns consisting of one or two bounded-cavity solitons are illustrated in Figs. 6 and 7, respectively. When two cavity solitons are separated initially by a distance on the order of the wavelength associated with the modulational instability, they repel each other, and,

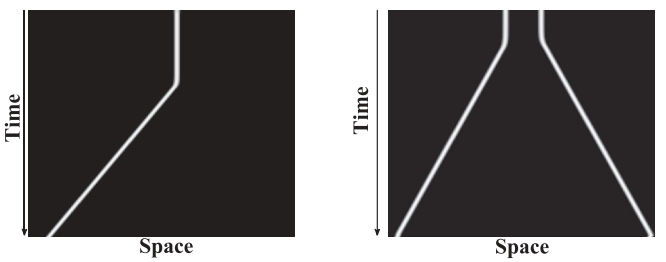


FIG. 6. Space-time map of a moving-cavity soliton solution of Eq. (5) in 1D. Left: single-cavity solitons; right: two-cavity solitons. Parameters are $p = -0.9$, $d = -1.5$, $a = 0.75$, $y = -0.5$, $\eta = -0.15$, and $\tau = 15$.

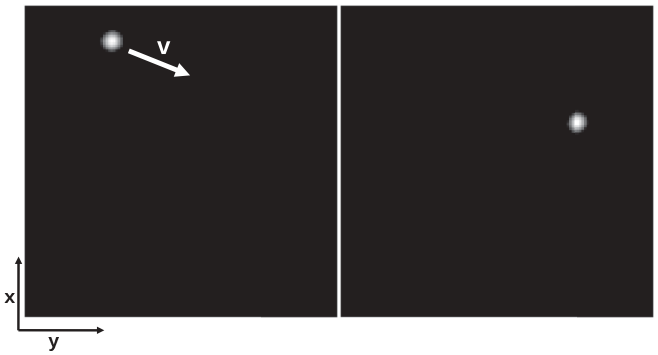


FIG. 7. Moving 2D cavity soliton solution of Eq. (5). Parameters are the same as in Fig. 6. The size of the system is 128 × 128.

therefore, start to move with equal but opposite velocities as shown in Fig. 8. Localized patterns consisting of a larger number of cavity solitons exhibit a similar behavior (see Fig. 9). The results shown in Figs. 6–9 have been obtained by numerical simulations of the generalized delayed Swift-Hohenberg equation (5) with periodic boundary conditions.

### B. Drift instability threshold and the velocity of the moving-cavity soliton

We have shown that below the drift instability threshold, the modified SH equation Eq. (5) admits stationary localized patterns involving either an odd or an even number of cavity solitons. In this section, we discuss the spontaneous motion of cavity solitons induced by the delayed feedback. We calculate the threshold value of the feedback strength above which cavity solitons start to move in an arbitrary direction and derive an expression for the velocity of the cavity soliton. By presenting the results of the numerical simulations of the full dynamical model Eqs. (1) and (2), we demonstrate that the existence of 2D moving-cavity solitons is not restricted to the nascent bistability regime but can also occur far from that regime.

The analytical expression for the drift instability threshold was derived in Ref. [26] in the case of the variational Swift-Hohenberg equation with the delay describing the passive nonlinear cavity. Let us first rewrite Eq. (5) in the form

$$\partial_t u = y - u(p' + u^2) + \eta[u(t-\tau) - u] + \left(d - \frac{5u}{2}\right)\nabla_\perp^2 u - \frac{(1-\alpha^2)}{4\alpha^2}\nabla_\perp^4 u - 2(\nabla_\perp u)^2, \quad (11)$$

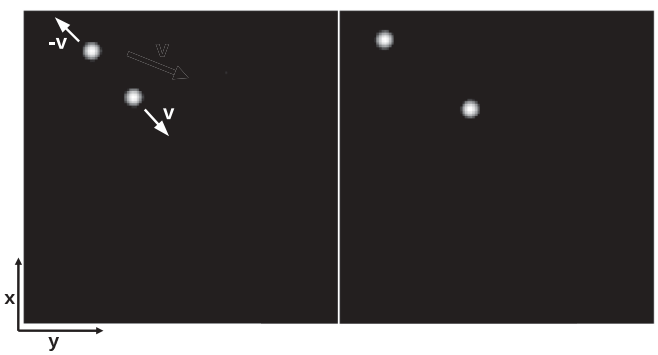


FIG. 8. Moving 2D cavity solitons solution of Eq. (5). Parameters are the same as in Fig. 6. The size of the system is 128 × 128.

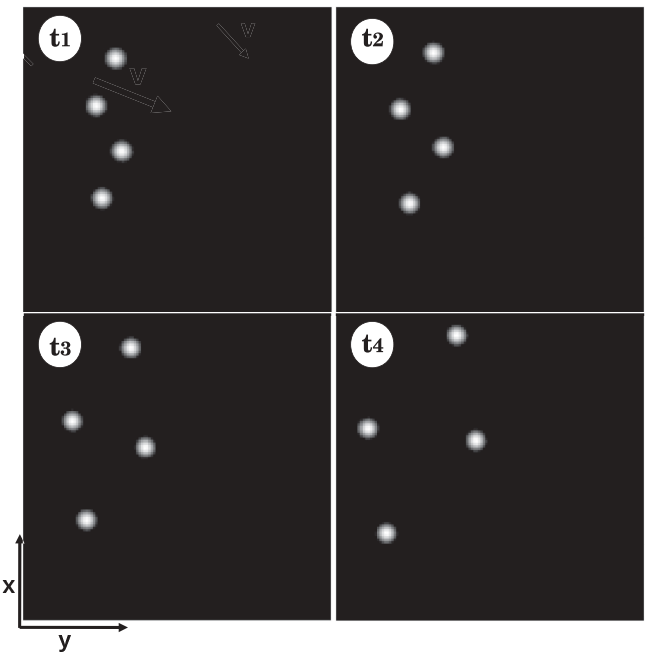


FIG. 9. Moving 2D localized pattern formed by four cavity solitons. Time sequence ($t_1 < t_2 < t_3 < t_4$) of the amplitude of the intracavity field solutions of the generalized delayed Swift-Hohenberg Eq. (5). Parameters are the same as in Fig. 6.

with $p' = p - \eta$. We assume that Eq. (11), without the term $\eta[u(t-\tau) - u]$, has a stable stationary radially symmetric soliton solution $u = u_0(|\mathbf{r}|)$. Stability of this solution means all the solutions $\Lambda$ of the following eigenvalue problem:

$$\mathcal{L}_\perp \phi = \Lambda \phi, \quad (12)$$

with the self-adjoint operator,

$$\mathcal{L}_\perp = -\left(p' + 3u_0^2 + \frac{5}{2}\nabla_\perp^2 u_0\right) + \left(d - \frac{5u_0}{2}\right)\nabla_\perp^2 - a\nabla_\perp^4$$

are real and negative except for a pair of zero eigenvalues, corresponding to the translational invariance of Eq. (11), $\Lambda_{1,2} = 0$. Since the term $\eta[u(t-\tau) - u]$ vanishes at any stationary solution, the stationary soliton $u_0(|\mathbf{r}|)$ is also a solution of Eq. (11) with $\eta \neq 0$. Let us substitute the slightly perturbed soliton solution $u(\mathbf{r},t) = u_0(|\mathbf{r}|) + \phi e^{\mu t}$ into Eq. (11). Then, linearizing it with respect to small perturbation $\phi$, we obtain

$$\mathcal{L}_\perp \phi = [\mu + \eta(1 - e^{\mu\tau})]\phi. \quad (13)$$

From Eqs. (12) and (13), we see that, for $\eta \neq 0$, the stability of cavity soliton solution $u_0$ requires that the real parts of all the solutions $\mu$ of the equation,

$$\mu + (1 - e^{\mu\tau})\eta = \Lambda \quad (14)$$

must be nonpositive for all $\Lambda$ satisfying Eq. (12). In particular, for the twofold degenerate eigenvalue $\Lambda_{1,2} = 0$, assuming that $|\mu| \ll 1$ and expanding Eq. (14) up to the second-order terms in $\mu$, we get two real solutions,

$$\mu_{1,2} = \frac{2(\eta\tau + 1)}{\eta\tau^2}, \quad \mu_{3,4} = 0, \quad (15)$$

where zero solutions $\mu_{3,4}$ are associated with the translational symmetry of the model equations and $\mu_{1,2}$ change their sign at the drift instability point $\eta\tau = -1$. At this point, where Eq. (14) has the fourfold degenerate solution $\mu_{1,2,3,4} = 0$, the stationary soliton solution loses stability, and the uniformly moving soliton solution bifurcates from the stationary one. According to Eq. (15), the stationary soliton is stable for $-1/\tau < \eta < 0$ and becomes unstable for $\eta\tau < -1$. The velocity of the moving single-cavity soliton can be estimated by performing an expansion in terms of a small parameter $\zeta$, which measures the distance from the drift instability threshold $\eta\tau = -1 - \zeta^2$. Let us look for a solution to Eq. (11) in the form of a uniformly moving-cavity soliton,

$$u(\mathbf{r},t) = u_0(\mathbf{R}) + \zeta^3 \delta u(\mathbf{R}) + \cdots, \quad \mathbf{R} = \mathbf{r} - \mathbf{v}t,$$

where $u_0$ is the stationary soliton solution evaluated at the drift instability point, $\mathbf{v} = \zeta \mathbf{V}$ is the soliton velocity, and $\delta u$ is the correction to the soliton shape due to its motion. Plugging this expression into Eq. (5), using the expansion $u_0(\mathbf{R} - \zeta V\tau) = u_0(\mathbf{R}) - \zeta V\tau u_1(\mathbf{R}) + (\zeta V\tau)^2 u_2(\mathbf{R})/2 - (\zeta V\tau)^3 u_3(\mathbf{R})/6 + \cdots$, where $V = |\mathbf{V}|$ and $u_p = (\mathbf{V}\cdot\nabla_\perp u_{p-1})/V$ $(p = 1$–$4)$, and collecting third order in $\zeta$, we obtain the following inhomogeneous problem:

$$\mathcal{L}_\perp \delta u = -V u_1 + \frac{\eta}{6}(V\tau)^3 u_3. \tag{16}$$

According to the solvability condition, the right-hand side of this equation should be orthogonal to the translational neutral modes $\phi_{x,y} = \partial_x u_0, \partial_y u_0$. By multiplying Eq. (16) with the linear combination of these modes $\mathbf{V}\cdot\nabla_\perp u_0/V \equiv u_1$ and integrating over 2D space, we obtain the equation for the cavity soliton velocity,

$$V\left(\int_{-\infty}^{+\infty} u_1^2 dx\, dy - \frac{\eta}{6} V^2\tau^3 \int_{-\infty}^{+\infty} u_1 u_3 dx\, dy\right) = 0. \tag{17}$$

A nontrivial solution of Eq. (17) is given by

$$v = \zeta V = \frac{Q}{\tau}\sqrt{-(1+\eta\tau)}, \quad \text{with} \quad Q = \sqrt{6\frac{\int_{-\infty}^{+\infty} u_1^2 dx\, dy}{\int_{-\infty}^{+\infty} u_2^2 dx\, dy}}, \tag{18}$$

where the relation $\int_{-\infty}^{+\infty} u_1 u_3 dx\, dy = -\int_{-\infty}^{+\infty} u_2^2 dx\, dy$ is used, which is obtained by integration by parts. The expression for the soliton velocity (18) coincides with that obtained earlier for the case of the variational Swift-Hohenberg equation [26], which describes a driven passive nonlinear cavity filled with two-level atoms. This expression is valid not only for a single-cavity soliton, but also for any localized patterns. The spatial form of the pattern affects only the factor $Q$ in Eq. (18), which can be calculated numerically. In particular, for the parameter values $y = -0.35$, $p = -0.7$, $d = -1.2$, and $a = 0.75$, we obtain $Q = 1.44$. The dependence of the soliton velocity on the time delay calculated using Eq. (18) is plotted for a fixed value of the feedback strength in Fig. 10. It is seen that the curve of the velocity has a maximum at $\tau = -2/\eta$, which corresponds to the maximal velocity $v_{\max} = -Q\eta/2$.

Moving-cavity solitons can be observed not only in the nascent optical bistability regime, but also far away from this regime. This is illustrated by Fig. 11, which was obtained by numerical integration of model Eqs. (1) and (2) using the

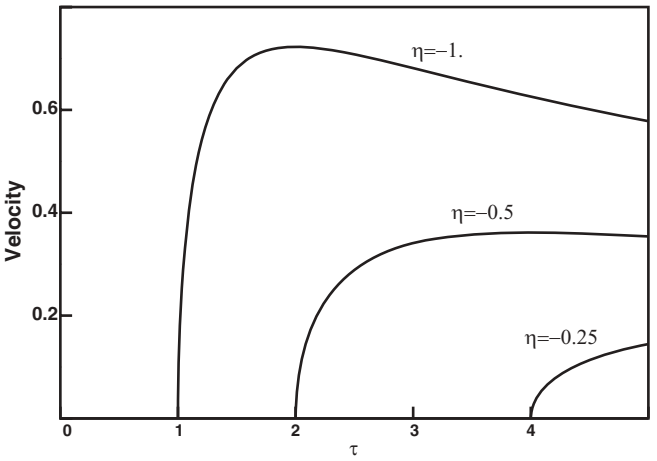


FIG. 10. Velocity of the moving-cavity soliton as a function of the time delay $\tau$ for different values of the delayed feedback strength $\eta$.

Runge-Kutta method together with the fast Fourier transform. The boundary conditions were periodic in transverse directions. From Fig. 11, it is seen that a single-cavity soliton exhibits a motion in an arbitrary direction in the $(x,y)$ plane due to the presence of delayed feedback. Noteworthy is the fact that, in the absence of delayed feedback, cavity solitons were observed experimentally in broad area VCSELs both below [7,41] and above [42] the lasing threshold.

## V. CONCLUSIONS AND PERSPECTIVES

In conclusion, we have shown that close to the nascent bistability threshold, the space-time dynamics of a broad area VCSEL, operating below the lasing threshold and subject to optical injection, is described by a generalized delayed Swift-Hohenberg equation. We showed that, in one transverse dimension, stationary-cavity solitons exhibited a clustering behavior in the pinning range of parameters where spatially

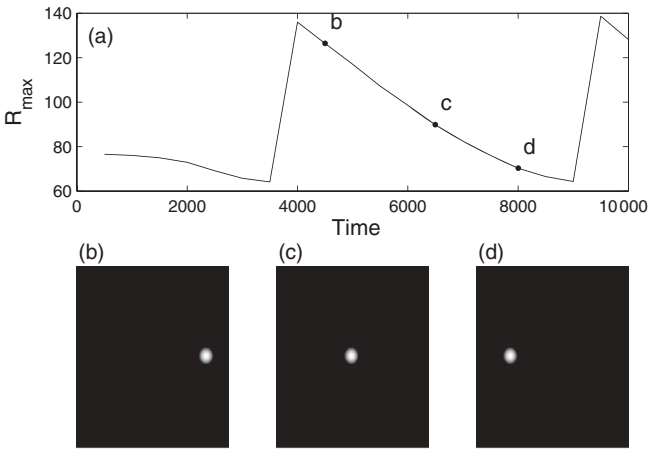


FIG. 11. Time evolution of the spatially localized 2D solution $|E(x,y,t)|^2$ of Eqs. (1) and (2). (a) Time evolution of the radius vector $R_{\max}$ of the peak of the cavity soliton. (b)–(d) Snapshots of the optical power distribution at the points indicated in (a). The parameter values are as follows: $\theta = -2$, $\alpha = 5$, $C = 0.45$, $I = 2$, and $\gamma' = 0.05$, $E_i = 0.8$. The feedback strength and phase are given by $\xi = 3$ and $\psi = 0.1$, respectively.

homogeneous and periodic solutions were both linearly stable. In this range, we constructed a snaking bifurcation diagram associated with stationary-cavity solitons. We demonstrated that one- and two-dimensional cavity solitons exhibited a drift instability, leading to a spontaneous motion in an arbitrary direction. We estimated the threshold of this instability and the velocity of the moving-cavity solitons. In two dimensions, the motion of two-cavity solitons was studied numerically. Finally, numerical simulations of the original models (1) and (2) showed that the described behavior was not limited to the nascent optical bistability regime but can also exist far away from this regime.

## ACKNOWLEDGMENTS

Fruitful discussions with Dr. S. V. Gurevich are gratefully acknowledged. A.V. acknowledges support from the SFB 787 project of the DFG, EU FP7 Marie Curie Initial Training Network PROPHET, Grant No. 264687, and the Program "Research and Pedagogical Cadre for Innovative Russia," Grant No. 2011-1.5-503-002-038. M.T. received support from the Fonds National de la Recherche Scientifique (Belgium). This research was supported by the Interuniversity Attraction Poles program of the Belgian Science Policy Office under Grant No. IAP P7-35 [43].

[1] M. Tlidi, M. Taki, and T. Kolokolnikov, Chaos **17**, 037101 (2007).
[2] N. Akhmediev and A. Ankiewicz, *Dissipative Solitons: From Optics to Biology and Medicine* (Springer-Verlag, Berlin/Heidelberg, 2008).
[3] T. Ackemann, W. J. Firth, and G. L. Oppo, Adv. At., Mol., Opt. Phys. **57**, 323 (2009).
[4] O. Descalzi, M. G. Clerc, S. Residori, and G. Assanto, *Localized States in Physics: Solitons and Patterns* (Springer, Berlin, 2010).
[5] H. G. Purwins, H. U. Bodeker, and S. Amiranashvili, Adv. Phys. **59**, 485 (2010).
[6] V. B. Taranenko, K. Staliunas, and C. O. Weiss, Phys. Rev. A **56**, 1582 (1997); Phys. Rev. Lett. **81**, 2236 (1998).
[7] S. Barland *et al*., Nature (London) **419**, 699 (2002).
[8] X. Hachair, L. Furfaro, J. Javaloyes, M. Giudici, S. Balle, J. Tredicce, G. Tissoni, L. A. Lugiato, M. Brambilla, and T. Maggipinto, Phys. Rev. A **72**, 013815 (2005).
[9] U. Bortolozzo, L. Pastur, P. L. Ramazza, M. Tlidi, and G. Kozyreff, Phys. Rev. Lett. **93**, 253901 (2004); M. G. Clerc, A. Petrossian, and S. Residori, Phys. Rev. E **71**, 015205 (2005); S. Residori *et al*., J. Opt. B **6**, S169 (2004).
[10] D. Bajoni, E. Semenova, A. Lemaître, S. Bouchoule, E. Wertz, P. Senellart, S. Barbay, R. Kuszelewicz, and J. Bloch, Phys. Rev. Lett. **101**, 266402 (2008).
[11] P. Genevet, S. Barland, M. Giudici, and J. R. Tredicce, Phys. Rev. Lett. **101**, 123905 (2008).
[12] X. Hachair, G. Tissoni, H. Thienpont, and K. Panajotov, Phys. Rev. A **79**, 011801(R) (2009).
[13] M. Tlidi, P. Mandel, and R. Lefever, Phys. Rev. Lett. **73**, 640 (1994); A. J. Scroggie *et al*., Chaos Solitons Fractals **4**, 1323 (1994); A. G. Vladimirov, J. M. McSloy, D. V. Skryabin, and W. J. Firth, Phys. Rev. E **65**, 046606 (2002); M. Tlidi, A. G. Vladimirov, and P. Mandel, IEEE J. Quantum Electron. **39**, 216 (2003).
[14] A. G. Vladimirov, R. Lefever, and M. Tlidi, Phys. Rev. A **84**, 043848 (2011).
[15] N. N. Rosanov, S. V. Fedorov, and A. N. Shatsev, Phys. Rev. Lett. **95**, 053903 (2005); N. A. Veretenov, N. N. Rosanov, and S. V. Fedorov, J. Opt. Quantum Electron. **40**, 253 (2008).
[16] C. O. Weiss, H. R. Telle, K. Staliunas, and M. Brambilla, Phys. Rev. A **47**, R1616 (1993).
[17] S. V. Fedorov, A. G. Vladimirov, G. V. Khodova, and N. N. Rosanov, Phys. Rev. E **61**, 5814 (2000).
[18] S. V. Gurevich, H. U. Bödeker, A. S. Moskalenko, A. W. Liehr, and H.-G. Purwins, Physica D **199**, 115 (2004).
[19] D. Turaev, M. Radziunas, and A. G. Vladimirov, Phys. Rev. E **77**, 065201(R) (2008).
[20] P. Coullet, J. Lega, B. Houchmanzadeh, and J. Lajzerowicz, Phys. Rev. Lett. **65**, 1352 (1990).
[21] D. Michaelis, U. Peschel, F. Lederer, D. V. Skryabin, and W. J. Firth, Phys. Rev. E **63**, 066602 (2001).
[22] K. Staliunas and V. J. Sanchez-Morcillo, Phys. Rev. E **72**, 016203 (2005).
[23] P. L. Ramazza, S. Ducci, and F. T. Arecchi, Phys. Rev. Lett. **81**, 4128 (1998); E. Louvergneaux, C. Szwaj, G. Agez, P. Glorieux, and M. Taki, *ibid*. **92**, 043901 (2004); F. Papoff and R. Zambrini, *ibid*. **94**, 243903 (2005); A. G. Vladimirov *et al*., Opt. Express **14**, 1 (2006); R. Zambrini and F. Papoff, Phys. Rev. Lett. **99**, 063907 (2007); Phys. Rev. E **73**, 016611 (2006); S. Coen, M. Tlidi, P. Emplit, and M. Haelterman, Phys. Rev. Lett. **83**, 2328 (1999).
[24] K. Staliunas and V. J. Sanchez-Morcillo, Phys. Rev. A **57**, 1454 (1998).
[25] M. Tlidi, P. Mandel, and M. Haelterman, Phys. Rev. E **56**, 6524 (1997); M. Tlidi and P. Mandel, Phys. Rev. A **59**, R2575 (1999).
[26] M. Tlidi, A. G. Vladimirov, D. Pieroux, and D. Turaev, Phys. Rev. Lett. **103**, 103904 (2009); M. Tlidi *et al*., Eur. Phys. J. D **59**, 59 (2010).
[27] Y. Tanguy, T. Ackemann, W. J. Firth, and R. Jager, Phys. Rev. Lett. **100**, 013907 (2008).
[28] P. V. Paulau, D. Gomila, T. Ackemann, N. A. Loiko, and W. J. Firth, Phys. Rev. E **78**, 016212 (2008).
[29] P. V. Paulau, D. Gomila, P. Colet, M. A. Matias, N. A. Loiko, and W. J. Firth, Phys. Rev. A **80**, 023808 (2009).
[30] P. V. Paulau, D. Gomila, P. Colet, N. A. Loiko, N. N. Rosanov, T. Ackemann, and W. J. Firth, Opt. Express **18**, 8859 (2010).
[31] B. Y. Rubinstein, A. A. Nepomnyashchy, and A. A. Golovin, Phys. Rev. E **75**, 046213 (2007); Y. Kanevsky and A. A. Nepomnyashchy, *ibid*. **76**, 066305 (2007); A. A. Golovin, Y. Kanevsky, and A. A. Nepomnyashchy, *ibid*. **79**, 046218 (2009); S. Coombes and C. R. Laing, Physica D **238**, 264 (2009); P. Ghosh, Phys. Rev. E **84**, 016222 (2011).

[32] K. Panajotov and M. Tlidi, Eur. Phys. J. D **59**, 67 (2010).

[33] S. Barbay, X. Hachair, T. Elsass, I. Sagnes, and R. Kuszelewicz, Phys. Rev. Lett. **101**, 253902 (2008); F. Haudin, R. G. Rojas, U. Bortolozzo, S. Residori, and M. G. Clerc, *ibid*. **107**, 264101 (2011).

[34] L. Spinelli, G. Tissoni, M. Brambilla, F. Prati, and L. A. Lugiato, Phys. Rev. A **58**, 2542 (1998).

[35] G. Kozyreff, S. J. Chapman, and M. Tlidi, Phys. Rev. E **68**, 015201 (2003); C. Durniak, M. Taki, M. Tlidi, P. L. Ramazza, U. Bortolozzo, and G. Kozyreff, *ibid*. **72**, 026607 (2005); G. Kozyreff and M. Tlidi, Chaos **17**, 037103 (2007).

[36] M. G. Clerc, A. Petrossian, and S. Residori, Phys. Rev. E **71**, 015205 (2005).

[37] E. Averlant, M. Tlidi, A. G. Vladimirov, H. Thienpont, and K. Panajotov, Proc. of SPIE **8432**, 84321D (2012).

[38] A. R. Campneys, Physica D **112**, 158 (1998); G. W. Hunt, G. J. Lord, and Champneys, Comput. Methods Appl. Mech. Eng. **170**, 239 (1999); P. Coullet, C. Riera, and C. Tresser, Phys. Rev. Lett. **84**, 3069 (2000).

[39] J. Burke and E. Knobloch, Chaos **17**, 037102 (2007); Y.-P. Ma, J. Burke, and E. Knobloch, Physica D **239**, 1867 (2010); D. J. B. Lloyd, B. Sandstede, D. Avitabile, and A. R. Champneys, SIAM J. Appl. Dyn. Syst. **7**, 1049 (2008); M. Tlidi and L. Gelens, Opt. Lett. **35**, 306 (2010).

[40] G. Kozyreff, M. Tlidi, A. Mussot, E. Louvergneaux, M. Taki, and A. G. Vladimirov, Phys. Rev. Lett. **102**, 043905 (2009).

[41] V. B. Taranenko, I. Ganne, R. J. Kuszelewicz, and C. O. Weiss, Phys. Rev. A **61**, 063818 (2000).

[42] X. Hachairet *et al*., IEEE J. Sel. Top. Quantum Electron. **12**, 339 (2006).

[43] photonics@be